

Probing Polaron Clouds by Rydberg Atom Spectroscopy

Marcel Gievers^{1,2,*}, Marcel Wagner³, and Richard Schmidt³

¹Arnold Sommerfeld Center for Theoretical Physics, Center for NanoScience, and Munich Center for Quantum Science and Technology, Ludwig-Maximilians-Universität München, 80333 Munich, Germany

²Max Planck Institute of Quantum Optics, 85748 Garching, Germany

³Institut für Theoretische Physik, Universität Heidelberg, 69120 Heidelberg, Germany

 (Received 6 June 2023; revised 24 October 2023; accepted 6 December 2023; published 31 January 2024)

In recent years, Rydberg excitations in atomic quantum gases have become a successful platform to explore quantum impurity problems. A single impurity immersed in a Fermi gas leads to the formation of a polaron, a quasiparticle consisting of the impurity being dressed by the surrounding medium. With a radius of about the Fermi wavelength, the density profile of a polaron cannot be explored using *in situ* optical imaging techniques. In this Letter, we propose a new experimental measurement technique that enables the *in situ* imaging of the polaron cloud in ultracold quantum gases. The impurity atom induces the formation of a polaron cloud and is then excited to a Rydberg state. Because of the mesoscopic interaction range of Rydberg excitations, which can be tuned by the principal numbers of the Rydberg state, atoms extracted from the polaron cloud form dimers with the impurity. By performing first principle calculations of the absorption spectrum based on a functional determinant approach, we show how the occupation of the dimer state can be directly observed in spectroscopy experiments and can be mapped onto the density profile of the gas particles, hence providing a direct, real-time, and *in situ* measure of the polaron cloud.

DOI: [10.1103/PhysRevLett.132.053401](https://doi.org/10.1103/PhysRevLett.132.053401)

Mixtures of quantum particles are ubiquitous in physics, ranging from neutron matter [1] and the BCS-BEC cross-over in atomic gases [2] to superconducting phases in solid-state physics [3]. Quantum mixtures have been investigated for many decades, but more recently, drastic progress in the controllability of experiments with ultracold atomic gases allows for new insights into a plethora of physical phenomena. In the limit of an extremely imbalanced quantum mixture, a single impurity is immersed in a Fermi gas. This leads to the formation of Fermi polarons, quasiparticles formed of gas particles which dress the impurity [4–7]. Even though many polaronic properties are understood to a great extent [4–29], a direct observation of the polaron dressing cloud in continuum systems has been out of reach.

Fermi polarons are generated by the short-range interaction between a Fermi gas and impurity particles, which in cold atoms can be tuned by Feshbach resonances. The size of the resulting polaron dressing cloud is of the order of the Fermi wavelength, i.e., $r_c \sim k_F^{-1}$. For typical densities of ultracold atoms, i.e., $\rho_0 = 10^{11}–10^{13} \text{ cm}^{-3}$, the relevant length scales lie in the suboptical regime, $r_c \sim 100–500 \text{ nm}$, which hinders gaining insight into the

real-space structure of these fundamentally important quasiparticles.

In this Letter, we demonstrate how to overcome this challenge enabling an *in situ* measurement of the polaron cloud in cold atom experiments. To this end, we propose a new measurement technique to explore the density profile around the impurity by use of atomic Rydberg states. Key to the idea is the use of the long-range interaction between the Rydberg atom and the bath particles. This interaction is generated by the outermost electron on the Rydberg orbit [30] and induces the formation of ultralong-range Rydberg molecules (ULRMs), i.e., deeply bound states of atoms inside the interaction potential [31–38]. Intriguingly, the extent of the Rydberg atoms of $r_{\text{Ryd}} = 50–500 \text{ nm}$ matches precisely the typical size of the polaron dressing cloud. Hence, by tuning the principal quantum numbers n_{Ryd} of the Rydberg excitation, the binding length of ULRMs is tuned through the polaron cloud (cf. Fig. 1). ULRMs can thus serve as a precision sensor inserted into the polaron cloud. The occupation of ULRMs is detected via a straightforward measurement of the *optical* linear response absorption and can be mapped onto the *suboptical* size of the polaron cloud. Because of its fermionic nature, our method differs from recent probing of a BEC with Rydberg impurities; as for the fermionic systems studied here, the number of particles in the Rydberg radius remains always small [37,39,40].

We calculate Rydberg absorption spectra in the presence of a polaron cloud around the impurity using a functional

Published by the American Physical Society under the terms of the [Creative Commons Attribution 4.0 International](https://creativecommons.org/licenses/by/4.0/) license. Further distribution of this work must maintain attribution to the author(s) and the published article's title, journal citation, and DOI. Open access publication funded by the Max Planck Society.

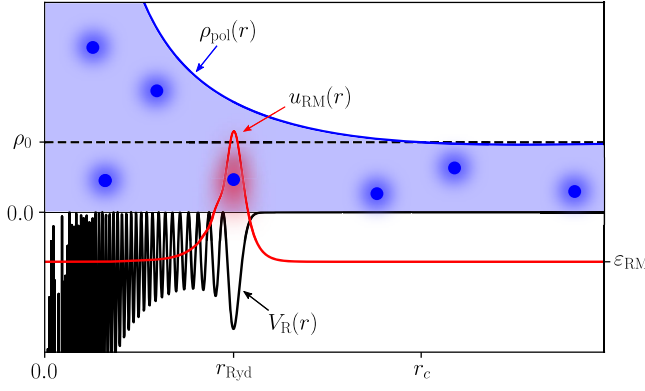


FIG. 1. A Rydberg atom in a polaron cloud. The bath density $\rho_{\text{pol}}(r)$ (blue line) is increased at the center compared to the background density ρ_0 (dashed line). The Rydberg potential $V_{\text{R}}(r)$ (black line) is tuned such that the outermost bound state $u_{\text{RM}}(r)$ (red line) at r_{Ryd} is situated near the polaron cloud radius r_c .

determinant approach [41–43]. The Rydberg blockade mechanism [44] ensures that our single-impurity calculations are applicable. While our approach becomes exact in the limit of heavy impurities immersed in a gas of lighter atoms, the idea of Rydberg sensing of polaron clouds can be extended to arbitrary mass ratios [45,46]. We show that, when the Rydberg excitation is immersed in a polaron cloud, the weight of the peak in the Rydberg absorption spectrum corresponding to the ULRM ground state gives direct access to the density evaluated at a distance r_{Ryd} from the impurity. This way, the complete density profile of polaron clouds, which so far eluded experimental observations, can be mapped out by use of a simple Rydberg spectroscopy experiment.

Model.—We consider a Fermi gas combined with a single charge-neutral and immobile impurity atom. The impurity can be brought into three states $\sigma \in \{0, 1, \text{R}\}$. For $\sigma = 0$, the impurity is not interacting with the bath particles. For $\sigma = 1$, the impurity interacts with the bath particles via a short-range interaction that induces the formation of a Fermi polaron [47]. For $\sigma = \text{R}$, the impurity is in the Rydberg state, which evokes the long-range interaction with the bath particles. The Hamiltonian reads:

$$\hat{H} = \hat{\mathbb{1}} \otimes \hat{H}_0 + \sum_{\sigma=1,\text{R}} |\sigma\rangle\langle\sigma| \otimes \hat{V}_\sigma, \quad (1a)$$

$$\hat{H}_0 = \sum_k \epsilon_k \hat{c}_k^\dagger \hat{c}_k, \quad \hat{V}_\sigma = \int_r V_\sigma(\mathbf{r}) \hat{c}_r^\dagger \hat{c}_r. \quad (1b)$$

Here, $\hat{c}_k^\dagger, \hat{c}_k$ are fermionic operators of the gas and $|\sigma\rangle$ is the state of the impurity. When the impurity is in the state $|\sigma\rangle$, the time evolution of the fermionic gas is given by the Hamiltonian $\hat{H}_\sigma = \hat{H}_0 + \hat{V}_\sigma$, acting only on the fermionic subspace.

We propose the following procedure. At the beginning, the impurity is in the noninteracting state $|0\rangle$ and the bath particles form a Fermi sea $|\text{FS}\rangle$, yielding the many-body state $|\psi(t_0)\rangle = |0\rangle \otimes |\text{FS}\rangle$. By a radio-frequency (rf) pulse, the impurity is then switched to the short-range interacting state, i.e., $|\psi(t_0 + 0^+)\rangle = |1\rangle \otimes |\text{FS}\rangle$. Time evolution leads to the formation of the polaron cloud around the impurity atom. After sufficiently long dephasing time, the system is well described by $|\psi(t_1)\rangle = |1\rangle \otimes |\text{pol}\rangle$. Finally, by driving an optical transition, the impurity atom is transferred to the Rydberg state, i.e., $|\psi(t_1 + 0^+)\rangle = |\text{R}\rangle \otimes |\text{pol}\rangle$. This way, the Rydberg atom is, by construction, exactly placed in the center of the polaron cloud as illustrated in Fig. 1.

We simulate the impurity in the $|1\rangle$ state by a delta potential with an s -wave scattering length a [41,48]. The potential in the $|\text{R}\rangle$ state, which is generated by scattering of the Rydberg electron with the bath particles, is given by [30]

$$V_{\text{R}}(\mathbf{r}) = \frac{2\pi\hbar^2 a_e}{m_e} |\psi_{n_{\text{Ryd}}}(\mathbf{r})|^2. \quad (2)$$

Here, $\psi_{n_{\text{Ryd}}}(\mathbf{r})$ is the wave function of an s -wave Rydberg electron with principal number n_{Ryd} and scattering length a_e between an electron and neutral atoms of the background gas [48]. Because of the nonlocal potential $V_{\text{R}}(\mathbf{r})$, there is a finite overlap between the polaron cloud and bound states inside $V_{\text{R}}(\mathbf{r})$ (cf. Fig. 1).

For the calculation of physical quantities, we use the functional determinant approach, which is a standard method for determining spectra [45]. Specifically, the density $\rho_\sigma(\mathbf{r}, t)$ around the impurity in state $|\sigma\rangle$ is obtained by a Klich formula [48,53,55]:

$$\rho_\sigma(\mathbf{r}, t) = \text{tr}[\hat{\rho}(t) \hat{c}_r^\dagger \hat{c}_r] = \langle \mathbf{r} | e^{-i\hat{h}_\sigma t} n_{\text{F}}(\hat{h}_0) e^{i\hat{h}_\sigma t} | \mathbf{r} \rangle, \quad (3)$$

where $n_{\text{F}}(\epsilon) = (\epsilon^{\beta(\epsilon-\mu)} + 1)^{-1}$ is the Fermi-Dirac distribution with inverse temperature β and chemical potential μ and we set $\hbar = 1 = k_{\text{B}}$. The single-particle operator \hat{h}_σ corresponds to the Hamiltonian of the gas particles \hat{H}_σ .

The absorption spectrum of the Rydberg atom inside the polaron is obtained from Fermi's golden rule,

$$\begin{aligned} A_{\text{pol}}(\omega) &= 2\pi \sum_f |\langle f | \text{pol} \rangle|^2 \delta[\omega - (E_f - E_i)] \\ &= 2\text{Re} \int_0^\infty dt e^{i\omega t} \langle \text{pol} | e^{i\hat{H}_1 t} e^{-i\hat{H}_{\text{R}} t} | \text{pol} \rangle, \end{aligned} \quad (4)$$

where the gas is initially in the polaron state $|\text{pol}\rangle$ with total energy E_i and $|f\rangle$ represent the complete set of final states of the gas in presence of the Rydberg impurity $|\text{R}\rangle$ with total energies E_f .

We obtain the absorption spectrum as the Fourier transform of the Ramsey signal [22,48], which is calculated as a

time-dependent Slater determinant [41,43,48]. Through \hat{H}_1 and \hat{H}_R , $A_{\text{pol}}(\omega)$ depends on both the Rydberg principal quantum number n_{Ryd} and the scattering length a of the polaron. In the following, we consider the system at zero temperature [56] and express physical quantities in terms of the Fermi momentum k_F and Fermi energy ε_F , respectively [48]. Still, our method is robust against finite temperature as it depends only on the weight of spectral peaks and not their widths [48].

Fermi polaron cloud.—Before turning to its observation, we first describe the formation of the polaron cloud in the initial state of the system. In particular, we are interested in the stationary density profile, which is established after a hold time $t_1 \gg 1/\varepsilon_F$ [48]. In that limit, the density profile Eq. (3) close to the impurity is well described by the ground state of the Hamiltonian \hat{H}_1 and given by

$$\rho_{\text{pol}}(\mathbf{r}) = \langle \mathbf{r} | n_F(\hat{h}_1) | \mathbf{r} \rangle. \quad (5)$$

Because of spherical symmetry, the density depends only on the distance to the impurity, i.e., $\rho_{\text{pol}} = \rho_{\text{pol}}(r)$.

Figure 2 shows the density of the polaron cloud as a function of the inverse dimensionless scattering length $(ak_F)^{-1}$ measured with respect to the background density, $\rho_0 = k_F^3/(6\pi^2)$. For $a < 0$, the single-particle wave functions are drawn toward the impurity, resulting in a density enhancement near $r = 0$. This enhancement is accompanied by Friedel-like oscillations farther away from the impurity [see also Fig. 2(b)]. On the contrary, for $a > 0$, the single-particle scattering wave functions are pushed away from the impurity. However, the bound state emerging at positive scattering length still leads to an overall enhancement of the density near the impurity [42]. Note that the particle density is formally divergent at $r = 0$, which is an artifact of the contact interaction and not present for physical finite-range potentials [48]. However, for all our considerations, the delta impurity is a valid approximation as the usual van der Waals length of the atoms is much shorter than the size of the Rydberg state. Importantly, the integrated number of particles in the polaron cloud converges to a well-defined, finite number, also in the limit of contact interaction.

We define the region with an increased particle density around the impurity as the *polaron cloud*. The size r_c of the polaron cloud, visualized by a green line in Fig. 2(a), is determined by the first crossing of $\rho_{\text{pol}}(r_c) = \rho_0$ and it is of the order of the Fermi wavelength.

The number of particles contributing to the polaron cloud N_c is given by the integrated number of excess atoms within the volume defined by r_c , i.e., $N_c = N_{\text{pol}}(r_c) - N_0(r_c)$ [48]. Note that the number of particles contributing to the polaron cloud is at most one particle despite the infinitely many particle-hole excitations required to obtain the exact many-body solution [57]. This is confirmed by a

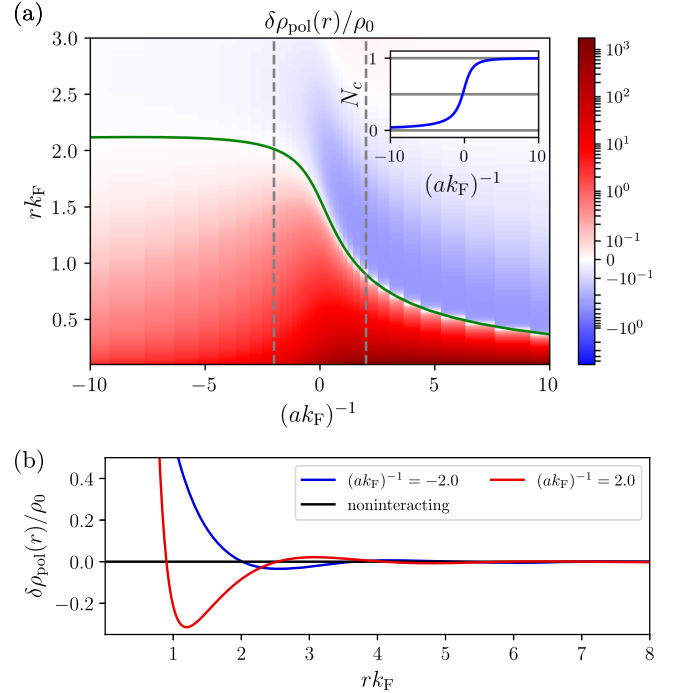


FIG. 2. (a) Polaron density profiles $\delta\rho_{\text{pol}}(r) = \rho_{\text{pol}}(r) - \rho_0$ in dependence on the inverse scattering lengths $(ak_F)^{-1}$ measured in terms of ρ_0 . The size of the polaron cloud r_c is marked in green. The integrated number of excess particles in the cloud N_c is shown in the inset. Note that the color plot is semilogarithmic. (b) Polaron cloud density for two exemplary scattering lengths marked as gray dashed lines in the upper plot.

thermodynamic consideration using Fumi's theorem [22,48]. However, although the number of contributing particles is small, it is the enormous density increase at the center that results in a significant effect in absorption spectroscopy in the presence of the Rydberg excitation.

We note that the real-time evolution of the polaron cloud formation can be obtained in a similar fashion by directly applying Eq. (3). While the corresponding absorption spectra, which then track the real-time formation of the polaron cloud, can also be calculated using linear response theory, in this Letter we focus on the quasistationary limit [cf. Eq. (5)].

Rydberg atom spectroscopy.—Let us now describe the Rydberg absorption spectra in the presence of a polaron cloud. The potential $V_R(r)$ in Eq. (2) features a pronounced minimum at the Rydberg radius r_{Ryd} (see Fig. 1). This minimum supports a spatially confined bound state leading to a prominent dimer peak in the absorption spectrum [32,33,38,43,44,48]. We refer to that state as the *Rydberg molecule (RM)* to differentiate it from higher excited bound states. The Rydberg radius r_{Ryd} can be tuned by the principal quantum number n_{Ryd} and is characteristic for the atomic species of the impurity (in our case ^{87}Rb).

A typical absorption spectrum calculated in the presence of the polaron cloud is shown in Fig. 3(a). The visible peaks

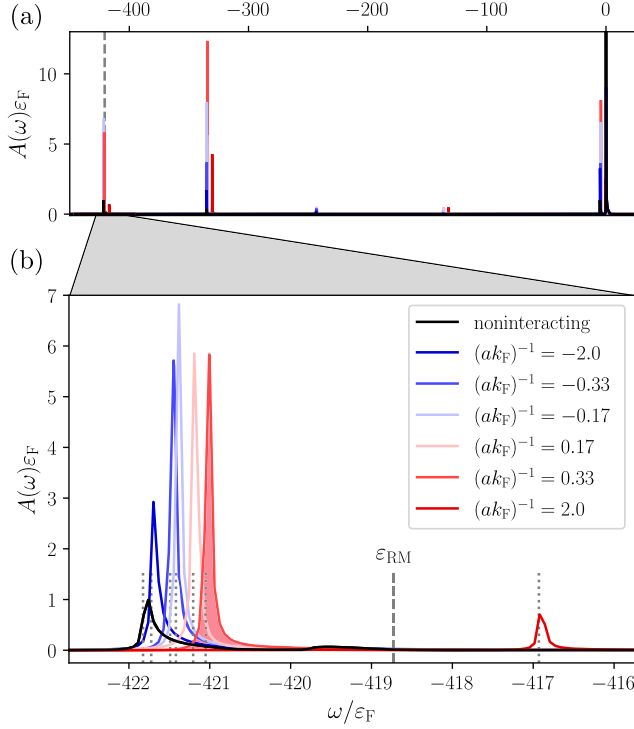


FIG. 3. (a) Absorption spectrum of a Rydberg impurity with $n_{\text{Ryd}} = 60$ generated in polarons of different inverse scattering lengths $(ak_{\text{F}})^{-1}$ at background density $\rho_0 = 5 \times 10^{11} \text{ cm}^{-3}$. The binding energy ε_{RM} is marked as a dashed gray line. (b) Magnification of the RM peak: Peak positions ω_{peak} Eq. (7) are marked by gray dotted lines. The red shaded region below the curve for $(ak_{\text{F}})^{-1} = 0.33$ indicates the value of the corresponding peak weight I_{pol} . The calculations are performed for a ^{87}Rb impurity in ^{40}K particles.

correspond to the various bound states between the Rydberg atom and bath particles. For $a = 0$, the density ρ_0 is spatially constant in the initial state and one recovers the results for a single Rydberg impurity in a Fermi gas [38,43]. Because of its good overlap with the scattering states of the Fermi gas, the RM with binding energy ε_{RM} (indicated by the dashed vertical line) has the largest oscillator strength.

For $a \neq 0$, a Fermi polaron is formed in the initial state. In this case the RM peak does not necessarily remain the most prominent peak of the spectrum. This can be understood from the increased density close to the impurity that causes bound states localized more closely to the impurity to have a larger overlap with the polaron's scattering states.

Looking closer at the RM response [cf. Fig. 3(b)], we observe two key changes in the spectrum that enable the spectroscopy of polarons: (a) the weight of the peaks is modified and (b) their position is shifted. In order to associate the weight of the RM peak with the polaron cloud density at distance r_{Ryd} , we perform an integral over a frequency window that encompasses the dimer peak [see exemplary shaded region in Fig. 3(b)]:

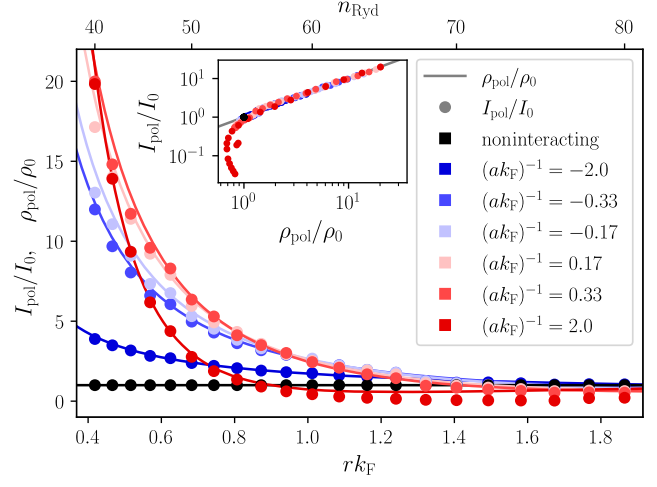


FIG. 4. Normalized density profiles $\rho_{\text{pol}}(r)/\rho_0$ Eq. (5) for polaron clouds formed at inverse scattering lengths $(ak_{\text{F}})^{-1}$ (solid lines) compared to the integrated dimer response $I_{\text{pol}}(r_{\text{Ryd}})/I_0(r_{\text{Ryd}})$ Eq. (6) (dots). The latter corresponds to the Rydberg radius through the respective principal numbers, i.e., $r_{\text{Ryd}}(n_{\text{Ryd}})$. We use a fixed $\rho_0 = 5 \times 10^{11} \text{ cm}^{-3}$. The inset shows the dependence between I_{pol}/I_0 and the densities ρ_{pol}/ρ_0 . Apart from deviations for small densities, the data points show a tight relation, which is underlined by the gray line marking identity. The calculations are performed for a ^{87}Rb impurity in ^{40}K particles.

$$I_{\text{pol}}(n_{\text{Ryd}}) = \int_{\text{peak}} d\omega A_{\text{pol}}(n_{\text{Ryd}}, \omega). \quad (6)$$

For absorption spectra at different principal numbers and scattering lengths, we calculate the integrated weight as a function of the principal number, i.e., $I_{\text{pol}}(n_{\text{Ryd}})$. Crucially, since n_{Ryd} is directly related to r_{Ryd} , these values are associated with the density ρ_{pol} at the respective distance. The comparison of $I_{\text{pol}}(n_{\text{Ryd}}) = I_{\text{pol}}(r_{\text{Ryd}})$ with $\rho_{\text{pol}}(r)$ is shown in Fig. 4, where we normalized the signal strength and density by the noninteracting values $I_0(r_{\text{Ryd}})$ and ρ_0 . We find striking agreement between the integrated weights of the dimer peaks $I_{\text{pol}}(r_{\text{Ryd}})/I_0(r_{\text{Ryd}})$ and the densities $\rho_{\text{pol}}(r)/\rho_0$. The strong correlation between both quantities is further analyzed in the inset of Fig. 4. Especially for larger density values, the mapping from absorption response to polaron cloud densities works exceptionally well. As our procedure depends only on the integrated spectral weight, it is robust against broadening effects on the spectrum, i.e., finite temperatures [45,48], mobile impurities [46], and the finite lifetime of the Rydberg excitation [35].

Our predictions are made in units of the Fermi momentum, i.e., $r_c = r_c(k_{\text{F}})$. Hence, another way of tuning the location of the Rydberg radius r_{Ryd} relative to the polaron cloud is by changing the overall density of the medium $\rho_0 = k_{\text{F}}^3/(6\pi^2)$. The discussion of density profiles reconstructed using this

alternative method is provided in the Supplemental Material [48].

The shifted positions of the RM peaks (cf. Fig. 3) allow us to directly measure the energy of attractive Fermi polarons. The peak position is given by

$$\omega_{\text{peak}} = \varepsilon_{\text{RM}} - E_{\text{pol}}(a) + E_{\text{pol,R}}(n_{\text{Ryd}}), \quad (7)$$

which makes the argument evident. First, the RM peak energy is reduced by the energy of the attractive polaron $E_{\text{pol}}(a)$ in the initial state [22]. Second, the presence of the Rydberg impurity shifts the single-particle energies of the Fermi gas itself once more, resulting in an additional polaron shift given by $E_{\text{pol,R}}(n_{\text{Ryd}})$. It is quite noticeable that our absorption spectra thus simultaneously provide two complementary properties of the polaron: it resolves its energy as well as its real-space density profile.

Conclusion.—We have proposed a new technique for probing the dressing cloud of polarons using Rydberg spectroscopy. ULRMs are the key feature enabling the approach. They are formed at a specific distance from the impurity and lead to dimer peaks that can be uniquely identified in absorption spectra. When tuning the principal number n_{Ryd} of the Rydberg state, the location of the ULRM is changed and the integrated weight of its dimer peaks directly corresponds to the density of gas particles. While we focused on the case of Fermi polarons, our procedure is general and can be extended to mobile impurities featuring molaron states [58], and other correlated many-body states such as Bose polarons [59–62] or polarons created in BCS superfluids [63]. Thus, the proposed technique paves the way to completely new observations in experiments with ultracold atoms that can probe length scales beyond the optical regime in an *in situ* fashion.

Finally, by employing deeply bound states as a probe, the proposed spectroscopy allows for observing dynamics on timescales that are ultrafast compared to the typical scales of the underlying many-body system. This allows us, for example, to investigate the formation of the polaron cloud in real time. In theory, this can be simulated by considering the linear response to the switch-on of the impurity similar to pump-probe spectroscopy.

We thank Hossein Sadeghpour and Márton Kanász-Nagy for fruitful discussions. We acknowledge funding for M. G. from the International Max Planck Research School for Quantum Science and Technology (IMPRS-QST). M. W. and R. S. acknowledge support by the DFG Priority Programme of Giant Interactions in Rydberg Systems (GiRyd) and by the Deutsche Forschungsgemeinschaft under Germany’s Excellence Strategy EXC 2181/1–390900948 (the Heidelberg STRUCTURES Excellence Cluster). The numerical simulations were performed on the Linux clusters at the Leibniz Supercomputing Center.

*Corresponding author: m.gievers@lmu.de

- [1] M. Kutschera and W. Wójcik, *Phys. Rev. C* **47**, 1077 (1993).
- [2] W. Zwerger, *The BCS-BEC Crossover and the Unitary Fermi Gas* (Springer Science & Business Media, New York, 2011), Vol. 836.
- [3] J. R. Schrieffer and J. S. Brooks, *Handbook of High-Temperature Superconductivity* (Springer, New York, 2007).
- [4] N. V. Prokof’ev and B. V. Svistunov, *Phys. Rev. Lett.* **81**, 2514 (1998).
- [5] N. Prokof’ev and B. Svistunov, *Phys. Rev. B* **77**, 020408(R) (2008).
- [6] A. Schirotzek, C.-H. Wu, A. Sommer, and M. W. Zwierlein, *Phys. Rev. Lett.* **102**, 230402 (2009).
- [7] P. Massignan, M. Zaccanti, and G. M. Bruun, *Rep. Prog. Phys.* **77**, 034401 (2014).
- [8] F. Chevy, *Phys. Rev. A* **74**, 063628 (2006).
- [9] R. Combescot, A. Recati, C. Lobo, and F. Chevy, *Phys. Rev. Lett.* **98**, 180402 (2007).
- [10] C. Mora and F. Chevy, *Phys. Rev. A* **80**, 033607 (2009).
- [11] M. Punk, P. T. Dumitrescu, and W. Zwerger, *Phys. Rev. A* **80**, 053605 (2009).
- [12] S. Nascimbène, N. Navon, K. J. Jiang, L. Tarruell, M. Teichmann, J. McKeever, F. Chevy, and C. Salomon, *Phys. Rev. Lett.* **103**, 170402 (2009).
- [13] S. Zöllner, G. M. Bruun, and C. J. Pethick, *Phys. Rev. A* **83**, 021603(R) (2011).
- [14] M. Koschorreck, D. Pertot, E. Vogt, B. Fröhlich, M. Feld, and M. Köhl, *Nature (London)* **485**, 619 (2012).
- [15] C. Kohstall, M. Zaccanti, M. Jag, A. Trenkwalder, P. Massignan, G. M. Bruun, F. Schreck, and R. Grimm, *Nature (London)* **485**, 615 (2012).
- [16] A. Wenz, G. Zürn, S. Murmann, I. Brouzos, T. Lompe, and S. Jochim, *Science* **342**, 457 (2013).
- [17] J. Vlietinck, J. Ryckebusch, and K. Van Houcke, *Phys. Rev. B* **87**, 115133 (2013).
- [18] W. Ong, C. Cheng, I. Arakelyan, and J. E. Thomas, *Phys. Rev. Lett.* **114**, 110403 (2015).
- [19] R. S. Christensen and G. M. Bruun, *Phys. Rev. A* **91**, 042702 (2015).
- [20] F. Scazza, G. Valtolina, P. Massignan, A. Recati, A. Amico, A. Burchianti, C. Fort, M. Inguscio, M. Zaccanti, and G. Roati, *Phys. Rev. Lett.* **118**, 083602 (2017).
- [21] M. Sidler, P. Back, O. Cotlet, A. Srivastava, T. Fink, M. Kroner, E. Demler, and A. Imamoglu, *Nat. Phys.* **13**, 255 (2017).
- [22] R. Schmidt, M. Knap, D. A. Ivanov, J.-S. You, M. Cetina, and E. Demler, *Rep. Prog. Phys.* **81**, 024401 (2018).
- [23] Z. Yan, P. B. Patel, B. Mukherjee, R. J. Fletcher, J. Struck, and M. W. Zwierlein, *Phys. Rev. Lett.* **122**, 093401 (2019).
- [24] N. Darkwah Oppong, L. Riegger, O. Bettermann, M. Höfer, J. Levinsen, M. M. Parish, I. Bloch, and S. Fölling, *Phys. Rev. Lett.* **122**, 193604 (2019).
- [25] G. Ness, C. Shkedrov, Y. Florshaim, O. K. Diessel, J. von Milczewski, R. Schmidt, and Y. Sagi, *Phys. Rev. X* **10**, 041019 (2020).
- [26] H. S. Adlong, W. E. Liu, F. Scazza, M. Zaccanti, N. D. Oppong, S. Fölling, M. M. Parish, and J. Levinsen, *Phys. Rev. Lett.* **125**, 133401 (2020).
- [27] I. Fritsche, C. Baroni, E. Dobler, E. Kirilov, B. Huang, R. Grimm, G. M. Bruun, P. Massignan, *Phys. Rev. A* **103**, 053314 (2021).

- [28] P. E. Dolgirev, Y.-F. Qu, M. B. Zvonarev, T. Shi, and E. Demler, *Phys. Rev. X* **11**, 041015 (2021).
- [29] F. Scazza, M. Zaccanti, P. Massignan, M. M. Parish, and J. Levinsen, *Atoms* **10**, 55 (2022).
- [30] N. Y. Du and C. H. Greene, *Phys. Rev. A* **36**, 971 (1987).
- [31] C. H. Greene, A. S. Dickinson, and H. R. Sadeghpour, *Phys. Rev. Lett.* **85**, 2458 (2000).
- [32] V. Bendkowsky, B. Butscher, J. Nipper, J. P. Shaffer, R. Löw, and T. Pfau, *Nature (London)* **458**, 1005 (2009).
- [33] B. Butscher, J. Nipper, J. B. Balewski, L. Kukota, V. Bendkowsky, R. Löw, and T. Pfau, *Nat. Phys.* **6**, 970 (2010).
- [34] B. J. DeSalvo, J. A. Aman, F. B. Dunning, T. C. Killian, H. R. Sadeghpour, S. Yoshida, and J. Burgdörfer, *Phys. Rev. A* **92**, 031403(R) (2015).
- [35] F. Camargo, J. D. Whalen, R. Ding, H. R. Sadeghpour, S. Yoshida, J. Burgdörfer, F. B. Dunning, and T. C. Killian, *Phys. Rev. A* **93**, 022702 (2016).
- [36] F. Camargo, R. Schmidt, J. D. Whalen, R. Ding, G. Woehl, Jr., S. Yoshida, J. Burgdörfer, F. B. Dunning, H. R. Sadeghpour, E. Demler, and T. C. Killian, *Phys. Rev. Lett.* **120**, 083401 (2018).
- [37] K. S. Kleinbach, F. Engel, T. Dieterle, R. Löw, T. Pfau, and F. Meinert, *Phys. Rev. Lett.* **120**, 193401 (2018).
- [38] J. D. Whalen, S. K. Kanungo, R. Ding, M. Wagner, R. Schmidt, H. R. Sadeghpour, S. Yoshida, J. Burgdörfer, F. B. Dunning, and T. C. Killian, *Phys. Rev. A* **100**, 011402(R) (2019).
- [39] M. Schlagmüller, T. C. Liebisch, H. Nguyen, G. Lothead, F. Engel, F. Böttcher, K. M. Westphal, K. S. Kleinbach, R. Löw, S. Hofferberth *et al.*, *Phys. Rev. Lett.* **116**, 053001 (2016).
- [40] C. Veit, N. Zuber, O. A. Herrera-Sancho, V. S. V. Anasuri, T. Schmid, F. Meinert, R. Löw, and T. Pfau, *Phys. Rev. X* **11**, 011036 (2021).
- [41] M. Knap, A. Shashi, Y. Nishida, A. Imambekov, D. A. Abanin, and E. Demler, *Phys. Rev. X* **2**, 041020 (2012).
- [42] R. Schmidt, J. D. Whalen, R. Ding, F. Camargo, G. Woehl, Jr., S. Yoshida, J. Burgdörfer, F. B. Dunning, E. Demler, H. R. Sadeghpour, and T. C. Killian, *Phys. Rev. A* **97**, 022707 (2018).
- [43] J. Sous, H. R. Sadeghpour, T. C. Killian, E. Demler, and R. Schmidt, *Phys. Rev. Res.* **2**, 023021 (2020).
- [44] R. Löw, H. Weimer, J. Nipper, J. B. Balewski, B. Butscher, H. P. Büchler, and T. Pfau, *J. Phys. B* **45**, 113001 (2012).
- [45] M. Cetina, M. Jag, R. S. Lous, I. Fritsche, J. T. Walraven, R. Grimm, J. Levinsen, M. M. Parish, R. Schmidt, M. Knap *et al.*, *Science* **354**, 96 (2016).
- [46] W. E. Liu, J. Levinsen, and M. M. Parish, *Phys. Rev. Lett.* **122**, 205301 (2019).
- [47] We use here the terminology of polarons also in the infinite impurity mass limit where Anderson's orthogonality leads formally to a vanishing polaron quasiparticle weight [22]. For the physics of the polaron cloud formation this is, however, not relevant here.
- [48] See Supplemental Material at <http://link.aps.org/supplemental/10.1103/PhysRevLett.132.053401> for additional details, which includes Refs. [22,30,41–43,49–54].
- [49] J. J. Sakurai and J. Napolitano, *Modern quantum mechanics*, revised edition (Addison-Wesley, Boston, 2011).
- [50] I. Bloch, J. Dalibard, and W. Zwerger, *Rev. Mod. Phys.* **80**, 885 (2008).
- [51] C. E. Burkhardt and L. J. Leventhal, The quantum defect, in *Topics in Atomic Physics* (Springer, New York, 2006), pp. 214–229, [10.1007/0-387-31074-6_11](https://doi.org/10.1007/0-387-31074-6_11).
- [52] M. T. Eiles, *Phys. Rev. A* **98**, 042706 (2018).
- [53] I. Klich, An elementary derivation of Levitov's formula, in *Quantum Noise in Mesoscopic Physics*, edited by Y. V. Nazarov (Springer Netherlands, Dordrecht, 2003), pp. 397–402.
- [54] R. S. Lous, I. Fritsche, M. Jag, B. Huang, and R. Grimm, *Phys. Rev. A* **95**, 053627 (2017).
- [55] K. Schönhammer, *Phys. Rev. B* **75**, 205329 (2007).
- [56] To be precise, we have run our calculations at $T = 0.001\epsilon_F$.
- [57] P. W. Anderson, *Phys. Rev. Lett.* **18**, 1049 (1967).
- [58] O. K. Diessel, J. von Milczewski, A. Christianen, and R. Schmidt, [arXiv:2209.11758](https://arxiv.org/abs/2209.11758).
- [59] N. B. Jørgensen, L. Wacker, K. T. Skalmstang, M. M. Parish, J. Levinsen, R. S. Christensen, G. M. Bruun, and J. J. Arlt, *Phys. Rev. Lett.* **117**, 055302 (2016).
- [60] M.-G. Hu, M. J. Van de Graaff, D. Kedar, J. P. Corson, E. A. Cornell, and D. S. Jin, *Phys. Rev. Lett.* **117**, 055301 (2016).
- [61] Z. Z. Yan, Y. Ni, C. Robens, and M. W. Zwierlein, *Science* **368**, 190 (2020).
- [62] L. A. Peña Ardila, N. B. Jørgensen, T. Pohl, S. Giorgini, G. M. Bruun, and J. J. Arlt, *Phys. Rev. A* **99**, 063607 (2019).
- [63] J. Wang, X.-J. Liu, and H. Hu, *Phys. Rev. Lett.* **128**, 175301 (2022).